13th International Symposium on Particle Image Velocimetry – ISPIV 2019
Munich, Germany, July 22-24, 2019

Tomo-PTV measurement of a drop impact at air-water interface

Thomas Steinmann[1*], Jérôme Casas[1], Patrick Braud[2], Laurent David[2]

[1] Institut de Recherche en Biologie de l'Insecte, IRBI UMR CNRS 7261, Tours, FRANCE

[2] Institut PPrime, UPR 3346, CNRS-Université de Poitiers-ENSMA, France

[*] thomas.steinmann@univ-tours.fr

Abstract

The evaluation of the complete energy balance for interfacial flow requires the correct estimation of free surface topography together and simultaneously with the flow velocity beneath the surface. To solve this problem, an extension of the tomographic PIV/PTV to the measurement of three-dimensionnal (3D) flow at the air/water interface during the fall of a controlled droplet is proposed. Our original setup allows us to monitor in real time the 3D position of fluorescent tracer particles both on the surface and in the bulk flow. To overcome the shadow effect due to the presence of wave at the interface, we illuminate the flow through the underside of a truncated squared pyramidal water tank. The shape of the water tank is chosen such that optical access can be established orthogonally through the walls. Four high speed cameras are focused on the illuminated volume of the flow through the four lateral sides of the pyramidal water tank. The images of the four cameras are analysed using 3D Lagrangian Particle Tracking Velocimetry (Shake the Box technique in Lavision Davis 8.4, Schanz et al. (2016)). This technique allows to track accurately particles at seeding densities comparable to the thresholds for tomographic PIV and to reduce greatly the number of ghost particles. The 3D local velocities are then obtained by interpolating vector volumes from the discrete particles. The evaluation of interface position and bulk flow velocities allows the determination of energy balance. From the surface topography we can determine the surface curvature and potential energies and the bulk flow velocities are used to derive the kinetic energy in the flow. These energies are then compared to the total potential energy of the droplet.

1 Introduction

Characterizing drop impact with liquid interfaces is of importance in various fields, from biology of pathogen transmission (Gilet and Bourouiba (2015)), physics of aerosol generation (Joung and Buie (2015)) to industrial applications as spray coating (Yarin (2006)).The phenomenology of drop impact is clearly described in the litterature, from the study of coalescence at sufficiently low velocity to the caracterization of the splashing regimes for larger drop impact velocities (Rein (1993), Rein (1996), Leng (2002), Agbaglah et al. (2015), Thoraval et al. (2016)). Depending on drop kinetic energy and ratios between drop inertia and curvature, gravitationnal or viscous forces, a drop impact on the surface of a deep pool can result in spreading, splashing, or bouncing. These physical phenomena result from the conversion of drop kinetic energy into surface potential and curvature energies and fluid kinetic energy. Recents studies have focused on the estimation of the rate of energy transfer during the drop impact. Zhang et al. (2019) developed a numerical model of energy conversion to analyze the effects of inertial, surface tension, gravitational and viscous forces during the crown evolution of the drop impact phenomena. Michon et al. (2017) proposed a systematic experimental study of the curvature and potential energies of cavities induced by drop impacts. They relate the magnitude of these energies to the subsequent jet dynamics. They derived these energies from the rough visualization of the shadows of drops impacting interfaces, and neglect the bulk flow kinetic energy. Their visualizations of drop impact provided them some informations on the maximal surface energy from the cavity shaping. Nevertheless, a systematic and complete energy balance requires the correct estimation of precise time resolved free surface topography together with flow velocity beneath the surface.

Non intrusive optical measurements methods, developed over the past twenty years, are particularly suitable to estimate interface topography over extended area. Moisy et al. (2009) developed an innovative

method, based on the capture, from above, of images of a random dot pattern at the bottom of a basin transmitted through the liquid interface. Changes in the topography of the liquid–air interface result in changes in the refracted dot pattern images. Cobelli et al. (2009) performed the measurement of free surface liquid deformation, by projecting a fringe on colored water (with an opaque-white dye). Aureli et al. (2011) have developed a method based on light absorption, which principles was based on the imaging of the back light through a free surface. The water is colored and functions as a variable-density filter. The calibration step consists in gradually increasing the level of fluid. More recently Wildeman (2018) developed a synthetic schlieren imaging method based on fast Fourier demodulation. The main novelty of this technique came from its use of a 2D checkerboard periodic pattern as a backdrop to the refractive interface.

The physical phenomena occuring at the free surface are also caracterized by conversions of flow kinetic energy and momemtum into potential and curvature energies. The estimation of this transfer of energy or momentum necessitates also the estimation of the three dimensional velocity of the fluid within the few millimeters below the water surface. Several techniques allow to measure simultaneously the velocity and the topography of an interface. Douxchamps et al. (2005) proceed to a stereoscopic and velocimetric reconstruction of the free surface topography by the imaging of floating tracers. They also proposed in the same paper a second indirect technique that exploits a Bernoulli relation to determine the interface topography from the horizontal velocity field acquired using a single camera. Fouras et al. (2008) and Ng et al. (2011) developed a technique based on the correlation of reference and refracted images of a laser sheet through an interface. They obtained simultaneous measurement on both the free surface topography and the velocity vector field of free surface flows. Turney et al. (2009) used a method based on a stereoscopic system which they termed three-dimensional interfacial particle image velocimetry (3D-IPIV). More recently Chatellier et al. (2013) adressed the problem of the combined determination of shape and velocity of moving free surfaces using a parametric method based on the cross-correlation of image pairs obtained from a calibrated stereoscopic vision system. Gomit et al. (2013) studied the apparent displacement between a reference and refracted images of a laser sheet through an interface viewed from two viewpoints. They obtained simultaneous measures of the free surface topography and the 2D velocity field beneath surface in the wake of a ship model.

These techniques allow one to estimate velocity together with surface deformation, but are limited to the estimation of the velocity in a slide area, i.e., in a laser sheet below the surface (Gomit et al. (2013)), or at the interface itself (Turney et al. (2009), Douxchamps et al. (2005)). Here we describe an application of the tomographic particle tracking velocimetry (Tomo-PTV) technique to the estimation of the three dimensionnal velocity field in a free surface flow, together with the estimation of the topography of the interface. We use the '*Shake the Box*' (*STB*) method (Schanz et al. (2016)), which is a Lagragian method of tracking of individual particles at high particle densities in a three dimensional volume.

We apply the *STB* method to the study of the impact of a water droplet on the air water interface. We focus our application of tomographic tracking to the particular regime of drop impact ($We = 250 - 300$) at which a small crater and crown are formed and a worthington jet is ejected after the collapsing of the crater. The method is applied to the estimation of an energy balance at the air-water interface after a drop impact. In the first part of this paper, we will start with a description of our measurement procedure, presenting our tomographic measurement setup, calibration procedure and surface topography and velocity field estimation. In a second part, we describe the droplet impact, its qualitative visualisation and the equation of the energy balance occuring after the drop impacts the air-water interface. In a third part, we describe the evaluation of the time resolved interface position and bulk flow velocities. It allows the determination of a complete energy balance in a control volume, together with the estimation of the flux of energies through the boundary of the volume. From the surface topography, we can determine the surface curvature and potential energies and the bulk flow velocities are used to derive the kinetic energy in the flow. The ability of the method to provide a complete energy balance is motivated by the comparison of these energies with the total kinetic energy of the droplet.

2 Tomographic measurement

2.1 Measurement setup

We performed the tomographic particle image tracking (Tomo-PTV) measurements of the surface flow produced after the impact of a falling water droplet at the water surface of a water tank ($200\times200\times150$ mm). This experimental measurement setup is illustrated in Figure 1.a and b. To overcome the shadow effect due to the presence of waves at the interface, we illuminate the flow through the underside of a truncated squared pyramidal water tank. The shape of the water tank is chosen such that an optical access to the surface can

be established orthogonally through the walls. A pulsed laser (Photonics Industries DM30, 527 nm) illuminated the measurement volume via a custom light guide that included three mirrors and a cylindrical lens that expanded the beam in two axis to fit the measurement volume size. The laser was operated at high average power (25 W) and the pulse width was 244 ns. The enlarged beam went eventually through a diaphragm to avoid a decrease of light homogeneity in the periphery of the beam. The measurement volume is visualized by four high-speed cameras (Phantom Miro 310) placed below the water tank. These four cameras acquired pictures at a rate of 1000 frame/s, with a resolution of 1280×800 pixels. They were mounted on "Scheimpflug" optical mounts together with Nikon macro Lens (focal lenght 200 mm), ensuring focus on the entire plane. We increased the focal ratio (f-number) of the four macro lens up to $f = 18$ to obtain a relatively large depth of field of 15 mm. The high speed cameras are focused on the illuminated volume of the flow through the four lateral sides of the pyramidal water tank. The particular orientation of the cameras together with their given depth of field and field of view results in the production of a truncated pyramidal measurement volume (40×40×18 mm) as illustrated in Figure 1.d.

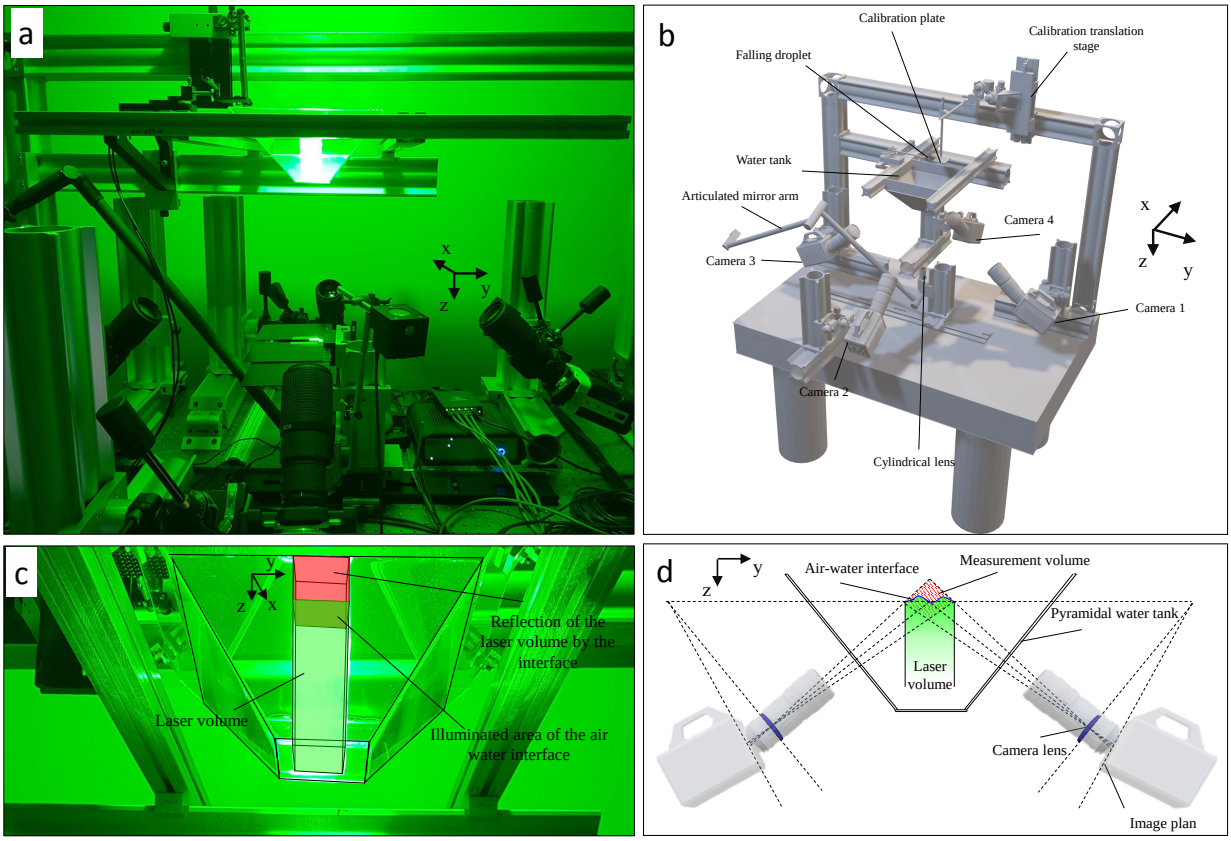

Figure 1: Tomographic PIV experimental setup used for the visualization of falling water droplets on an air-water interface. (a) Measurement setup. (b). Scheme of the measurement setup. (c). Close up view of the illumination of the air water interface. The enlarged laser beam, having a squared section, illumates the air-water interface from below through the lower face of the pyramidal water tank. This figure highlights the superposition of the volume of particules illuminated with its reflection by the interface (d). Illustration of the measurement volume. Given the particular orientation of the cameras, their fields of view and particular depths of field, we illustrate in two dimension the "diamond shape" overlap region of camera views, corresponding to our measurment volume (hatched in red). We estimate the particles position above and below the interface resting position.

We perform a seeding of the bulk flow with 22 μm polyamide fluorescent particles (Rhodamine B custom made, $\rho_p = 1,016 kg/dm^3$). We also used a cell strainer (SPL Life Science 93040) to deposit the fluorescent particles on the surface and allow them to remain suspended at the interface. The particular orientation angle between camera sensor and interface results in the appearance of a mirror image of the seeding particles above the interface, that superposes to the actual real particles below the interface on the sensor of each

camera, as illustrated in figure 1.c.

2.2 Calibration procedure

The need to track particles in the fluid and at the interface, below and above the resting position of the water surface ($z = 0mm$), imposed additional constraints on the calibration steps, notably the extension of the perpective calibration to heights over the resting position. These particular constraints do not apply to a measurement in a volume flow. Figure 2.a illustrates the procedure. The perspective calibration consists in the correct definition of the four mathematical relationship between the coordinates of a point in the three-dimensional space and the projection onto the image plane of each cameras. This calibration implies several records of the perspective view of a calibration target positionned at the center of the measurement volume. This calibration target is aligned carefully and defines the orientation of the coordinate system. In order to estimate correctly the velocity below and above the interface resting position ($z = 0mm$), we performed this calibration step in a water tank filled to a height equal to z = 9 mm, before emptying part of the tank to lower the surface at rest to z = 0. We moved the calibration target in 8 equidistant steps between $z = -12mm$ and $z = 9mm$ in the out of plane direction and recorded the projection of the target in the image plane of the 4 cameras.

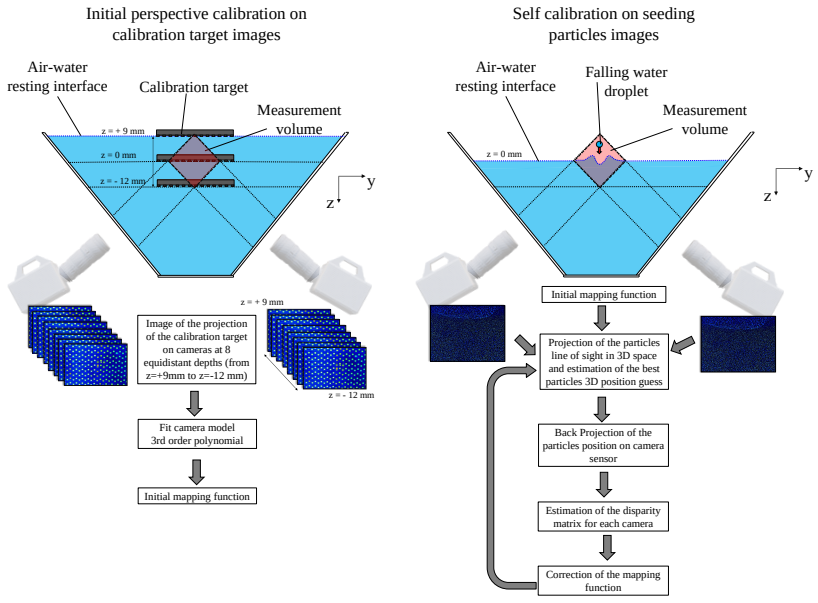

Figure 2: Explanation of the initial perspective calibration and self calibration steps. The initial calibration consists in eight records, by each of the four cameras, of the perspective view of a calibration target positionned at the center of the measurement volume. This calibration step is performed in a water tank filled to a height equal to z = 9 mm. We take images of the projection of the calibration target on the four cameras at 8 equidistant depths (from z=+9mm to z=-12 mm). We then fit the four 3^{rd} order polynomial camera models and obtain the initial mapping function. After draining some of the water from the water tank to lower the level of the resting surface to $z = 0mm$, we proceed to the self calibration on the acquisition of seeding particles images. Each camera records the images of seeding particles. Using the initial mapping function, we project the particles lines of sight in a three dimensional space to estimate the particles best 3D position. We then back-project the particles position on each camera sensors to estimate the matrix of disparity of each camera. This disparity matrix is then used to correct the previous mapping function. This self calibration step is repeated until the average disparity on all cameras is considered to be small enough.

We then drain a portion of the water to reduce the height of rest surface to $z = 0mm$ and proceed to the acquisition. In tomographic measurements, even the smallest vibration of the camera system could prevent the correct identification of particle positions, by preventing the precise crossing of the line of sight (LOS) of a particle from the four camera. That is why we also proceed to a volume self calibration (Figure 2.b).

Its purpose is to remove any residual calibration disparities using recorded image particles. The volume self calibration required two repeated and converging steps which are the calculation of the disparity of calibration and the correction of the calibration.

2.3 Tomographic tracking, velocity field calculation and estimation of the interface position

The superimposed reflection of a mirror image of the seeding particles above the interface produces noise and increases the risk to produce ghost particles (Figure 1.c). We will show that applying lagrangian tracking method to the evaluation of interfacial flow is better than the Algebraic volume reconstruction techniques (MART, SMART and SMTE).

The '*Shake the Box*' (*STB*) method, implemented in La Vision Davis 8.4 (Schanz et al. (2016)) is a three-dimensional particle tracking velocimetry method, originating in the classical tracking techniques, used for over 25 years. In these typical tracking techniques, the particle positions are determined using their projections on few images by triangulation for each time-step. The techniques rely on an individual treatment of every single snapshot of the particle distribution. The *STB* method uses a prediction of the particle positions at different subsequent time step to catch the accurate temporal evolution of the particle position. This prediction step reduces drastically the processing time and allows significant gains in accuracy due to an efficient suppression of ghost particles. The main novelty of the *STB* method is to introduce a refinement step during the process of prediction. In this step of the processing, the particles are somewhat displaced (shaked) to their correct position and intensity. All the particles are treated independently and successively. Shaking the particles consists in moving them in small steps in all directions of space, starting from their initial positions. This allows the elimination of the prediction error.

Figure 3 illustrates the comparative use of different techniques to reconstruct the volume of particles. This figure represents the projections of tomographic reconstructions along yz planes and shows that the use of classical algebraic reconstruction technique (Figure 3.a, Multiplicative Algebraic Reconstruction Technique, MART) results in the production of a large amount of ghost particles above the real air-water interface. We also show that even the iterative reconstruction method (Figure 3.b, Sequential Motion tracking Enhanced SMART, SMTE) does not prevent the lost of energy put into the ghost particles. The large amount of ghost particles is due to superimposed reflection of a mirror image of the seeding particles. Figure 3.c illustrates the gain, in terms of ghost particles reduction, of the use of the tracking *STB* method compared to two volume reconstruction techniques.

From the lagragian tracks of particles, we can estimate both the time resolved eulerian velocity fields and the evolution of the interface topography with time. The process allowing us to obtain this information is illustrated in the figure 4. The eulerian 3D local velocity fields are obtained by interpolating vector volumes from the discrete particles lagragian position and velocities. The particle track data is converted to velocity data on a regular grid of 12 voxels for each time steps. The surface topography is obtained after the interpolation of tracked particles position along z-axis on a regular (x,y) grid, followed by a search of the local maxima for a given (x,y) position.

3 Droplet production and energy balance

In this section, we first describe an independent and preliminary analysis of a drop impact on water surface. This visualisation will be used to validate our tomographic reconstruction results. In a second section, we describe the expressions used to derive the energy balance.

3.1 Droplet production, impact visualisation and description

We used a drip-feed device to generate constant volume droplets falling from a height $h_d = 15cm$. We first visualized the drop impact with an independant experimental setup, consisting of a close-up high speed camera (1000 frames per second) and a macro lense (Nikon f=50mm) that allowed us to record the impact with a definition of 40 μm per pixel. Figure 5 shows the temporal evolution of the air-water interface topography after the impact. In this preliminary experiment, the droplet initial velocity is zero, the average radius of the droplet to be equal to $R_d = 2,2mm$. The droplet diameter $D_d = 2R_d = 4,4mm$ is larger than the capilary length : $l_c = \sqrt{\sigma/\rho g} = 2mm$, where $\sigma = 40.10^{-3}N/m = 40.10^{-3}J/m^2$ is the air-water surface tension, $\rho = 1000kg/m^3$ is the water density and $\mu = 1mPa.s$ is the water dynamic viscosity. The droplet's impact velocity was $V_i = 1,6m/s$. The total kinetic energy of the droplet was $E_k^d = 5,7.10^{-5}J$. This qualitative study

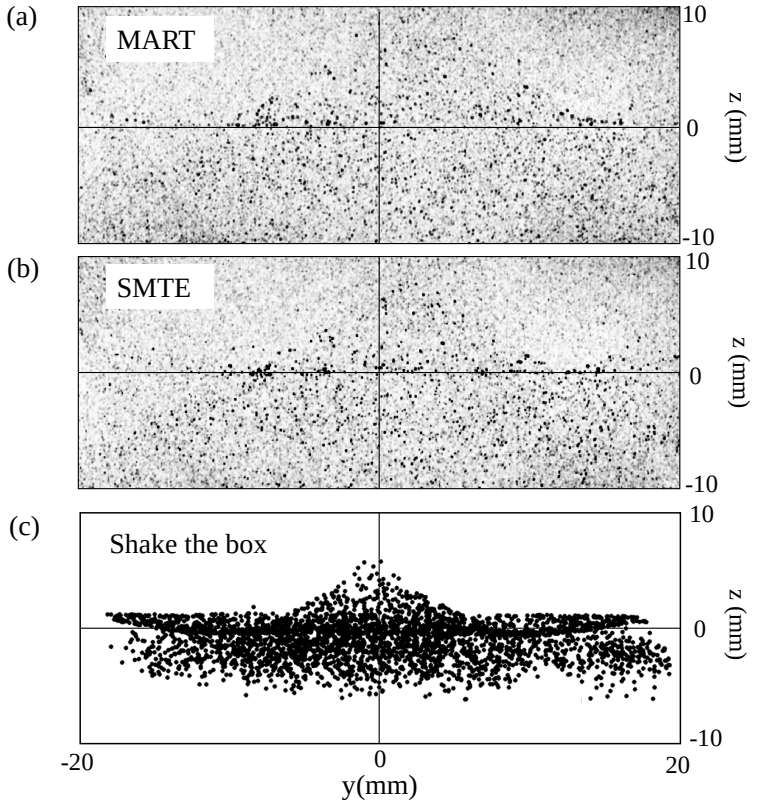

Figure 3: Comparaison of the projection of tomographic reconstructions and particles positions estimation by means of STB, at a time $t = 80ms$ after the impact of a water droplet at the position $x = 0mm$. We used three distinctive methods to reconstruct the particle volume. a. Projection along (yz) plane of the reconstructed volume of illuminated particles using the **MLOS SMART** method, b. Projection along (yz) plane of the reconstructed volume of illuminated particles using the **Sequential Motion tracking Enhanced SMART** and c. Projection along (yz) plane of the reconstructed particles position using the **Shake the box** method.

illustrates the appearance of a cavity resulting from the impact (between 7 and 20 ms). We determined the typical cavity dimensions (height $H = 7mm$ and width $2R = 14mm$). At this spatial scale we know that both gravity and capillarity forces rule the relaxation process, appearing in a second time. The cavity collapses between 30 and 40 ms and this collapse results in the emission of a back jet (between 50 and 80 ms). The jet will eventually fall back, producing a circular wave (between 100 and 130 ms).

In the Tomo-PTV experiment, the radius of the droplet falling from a height $h_d = 15cm$, was also equal to $R_d = 2,2mm$ and the impact velocity was $V_i = 1,6m/s$. The total kinetic energy of the droplet was $E_k^d = 5,7.10^{-5}J$.

3.2 Energy balance

During the impact of the water droplet with the interface, we suppose that the energy transfer results in the deformation of the surface, which gains an energy $E_s(t)$ and into a fluid displacement in the form of fluid kinetic energy $E_k^f(t)$. We can estimate the surface energy by using air-water interface topography data derived from (i) drop impact direct visualization and (ii) from tomo-PTV measurement. Using the high speed visualization presented in figure 5, we can only derived the maximal surface energy from the analysis of the geometry of the cavity shaping. Following Michon et al. (2017), we evaluate the surface energy as the sum of its gravitational potential energy $E_{pmax} = \pi/2\rho g H^2 R^2$ and its capillary energy $E_{cmax} = 2\pi\sigma HR$, where H and R are respectively the maximum depth and radius of the cavity ρ the water density and

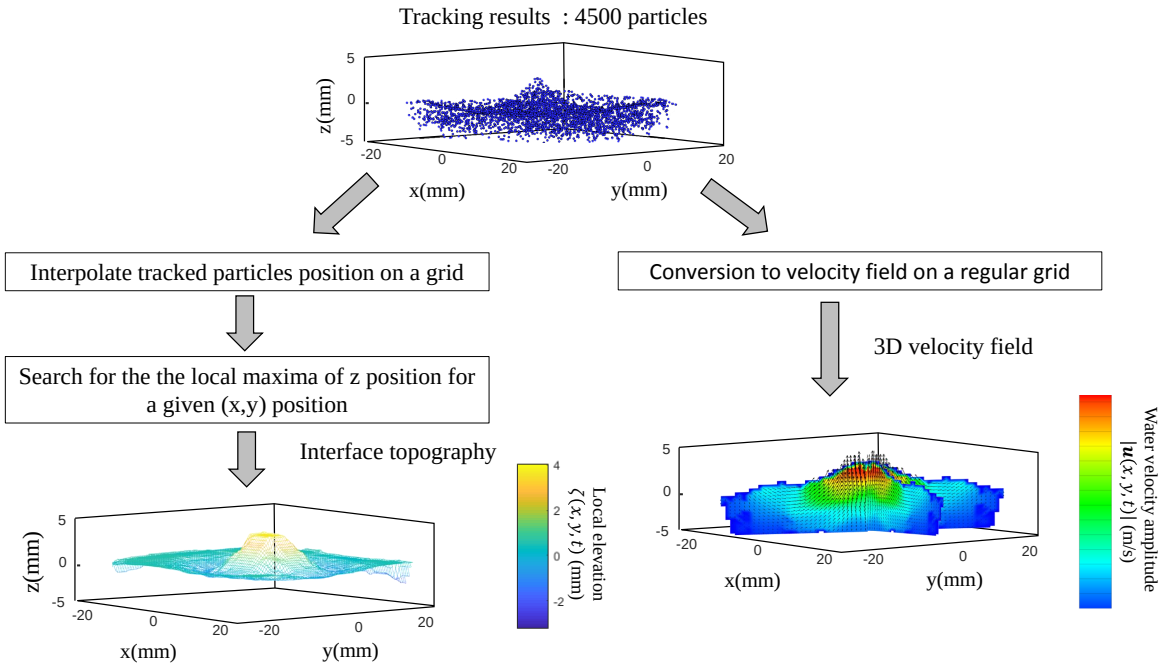

Figure 4: Illustration of the estimation of the local interface topography and the eulerian velocity field from tracked particle position at time $t = 80ms$.

$\sigma = 40.10^{-3} J/m^2$, is the surface tension. Using the surface topography measurement extracted from Tomo-PTV results, we evaluate the time resolved energy of the surface as the sum of its curvature (first term in the right hand equation) and gravitationnal (second term in the right hand equation) energies, that we can integrate on the entire air-water interface S:

$$E_s(t) = \frac{1}{2}\sigma \int_S dxdy|\nabla\zeta(t,x,y)|^2 + \frac{1}{2}\rho g \int_S dxdy\zeta^2(t,x,y)$$

where $\zeta(t,x,y)$ (m) is the time resolved air-water interface position and $\nabla\zeta(t,x,y)$ is the surface gradient. The curvature energy (first term in the right hand equation) corresponds to the change in the interface area when compared to the interface area at rest, multiplied by the surface tension $\sigma = 40.10^{-3} J/m^2$. The second term in the right hand equation is the gravitationnal energy of the interface. The energy is also transferred to the fluid in the form of fluid kinetic energy $E_k^f(t)$, being integrated on the entire control volume V_c :

$$E_k^f(t) = \frac{1}{2}\rho \int_{V_c} dxdydz\mathbf{u}(x,y,z,t)^2$$

With $\mathbf{u}(x,y,z,t)$ being the water velocity field. Ranging from -5 mm to +5 mm, our measurement domain is not deep enough to visualize the entire cavity. This forces us to consider carefully the flux of kinetic energy that will cross the bottom boundary (S_b) of our integration domain.

4 Results

4.1 Tomographic tracking, interface topography and calculation of velocity field

Figure 6.b shows the successive positions of tracked particles obtained after the *Shake the Box* analysis. When the drop impacts the surface, a cavity is first shaped, which then relaxes, giving rise to an upward vertical jet. From the lagragian estimation of the particles tracks we derived the time resolved interface

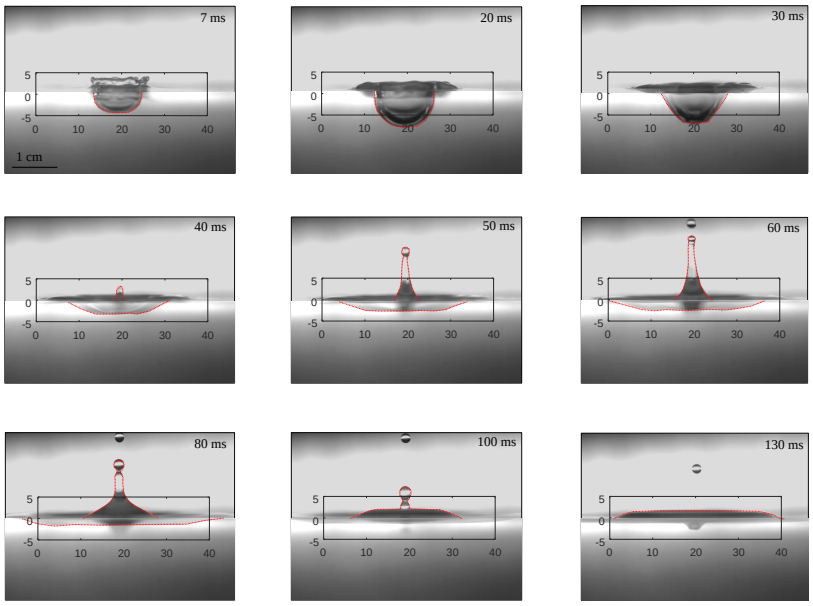

Figure 5: High speed camera visualization of the temporal evolution of a drop impact on a free surface of water ($D_d = 4.4mm$, $V_i = 1.6m/s$, $We = 280$, $E_k^d = 5.7.10^{-5}J$). After the drop impacts the surface, a cavity is formed and the cavity relaxes, giving rise to an upward vertical jet. The jet then fragments into droplets through successive end pinching events. The box superimposed on each image represents the extent of the tomographic reconstruction volume.

topography (Figure 6.c). The interface topography estimated from the surface particles position is compared to the direct visualization of the air-water interface (Figure 6.a). From the tracking results, we also derived the eulerian estimation of the velocity field in the flow below the air-water interface (Figure 7). In this figure we also illustrated the interface topography estimated from direct visualization of drop impact (Figure 5). We start the analysis at $t = 20$ ms after the drop impact on water surface. At the instant of impact both the large size of the droplet and its large velocity result in a large incurving of the interface and in a large decrease of particles concentration. We notice also a large decrease of particle detection at that instant.

We proceed to the description of the interface topography and flow velocity at the larger times. At 30 ms, the interface that was highly depressed starts to pull up and bounces up to a 5 mm height. The higher bouncing position of the interface is reached at 60 ms. After 60 ms, the interface relaxes by producing a circular wave. In terms of flow speed, at 30 ms, while the interface is highly depressed, the flow velocity is relatively low. The interface then pulls up the fluid , and the the flow velocity reaches its maximum around 50 ms.

4.2 Energy balance

The following energy analysis of both water interface and flow highlights the interplay and phase opposition of flow velocity and surface topography as described in the litterature. Zhang et al. (2019), for example, shows the energy conversion during the impact process of a drop upon film. At $t = 0$ ms the energy is totally contained in the droplet kinetic energy ($E_k^d = 5,7.10^{-5}J$). When the droplet hits the air-water interface, there is a transfer of droplet kinetic energy into surface energy, it creates a cavity. We have first evaluated the maximal surface energy E_{smax} from the cavity shaping visualized with direct high speed imaging presented in Figure 5. This energy is the sum of potential and curvature energies, and it reaches its maximum at $t = 20$ ms. It is equal to $E_{smax} = E_{pmax} + E_{cmax} = 3,7.10^{-5} + 1,2.10^{-5} = 4,9.10^{-5}J$. This maximal energy is lower than the initial droplet kinetic energy $E_k^d = 5,7.10^{-5}J$. It suggests that the totality of the kinetic energy is not converted into surface energy. We now show that at the same instant, the kinetic energy in the fluid is not zero. Figure 8.b shows the evolution of the balance between surface and fluid kinetic energies derived from the tomo-PTV experiment. Using the time resolved measure of the interface topography, we

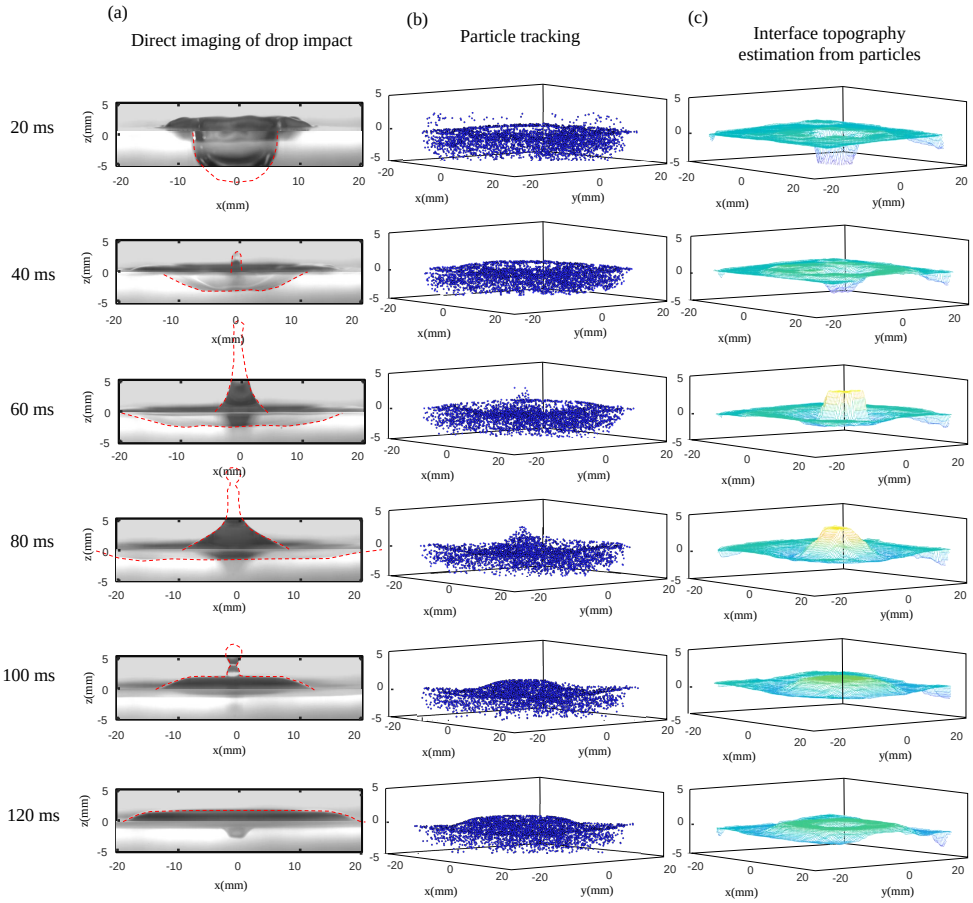

Figure 6: Time sequence of the interface topography and flow velocity after the impact of a water drop. ($V_i = 1,6m/s$, $D_d = 4,4mm$ $E_k^d = 5,7.10^{-5}J$, $We = 280$) (a) Direct visualization of the evolution of the air-water topography. (b) Temporal evolution of the tracked positions of particules. (c) Temporal evolution of the air water interface topography.

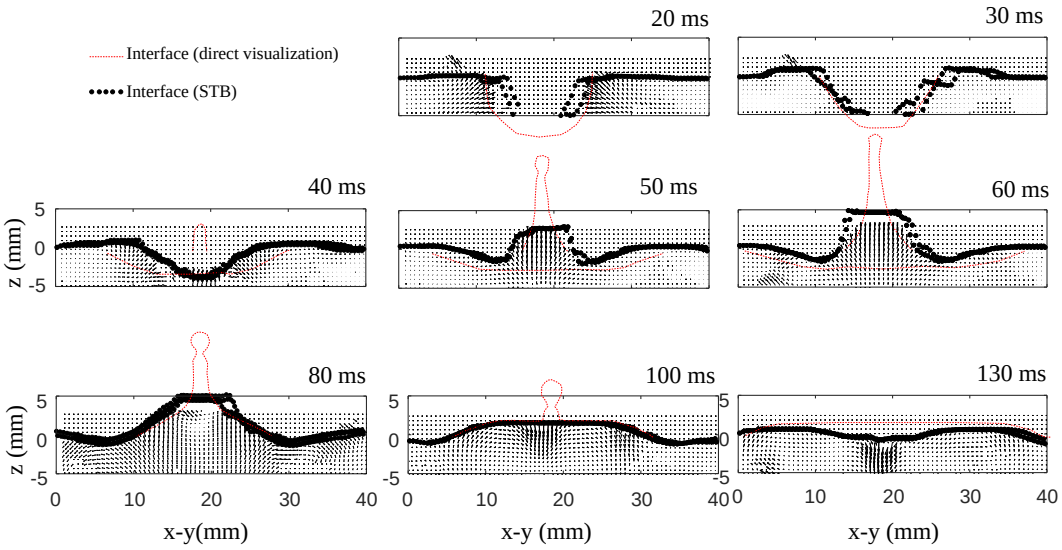

Figure 7: Temporal evolution of the flow velocity field and surface topography in the axisymmetric section crossing the impact point of the droplet. ($V_i = 1,6m/s$, $D_d = 4,4mm$ $E_k^d = 5,7.10^{-5}J$, $We = 280$). The dotted red line represents the interface estimated by the direct visualization of the drop impact. This direct visualization does not provide the topography of the median section of the interface, but rather an integrated information about the interface position on the impact volume.

estimate the potential energy and interface curvature energy, and using the 3D velocity field we estimate the kinetic energy of the flow. We can see that the surface energy derived from tomo-PTV experiment greatly underestimates the maximal surface energy derived from direct visualization at $t = 20$ ms (instant 0 in the figure 8.a). This divergence is explained by the large size of the droplet and by its large impact velocity. We estimate that a large part of its kinetic energy, transformed into curvature and potential gravitationnal energies has escaped through the lower boundary of the measurement volume.

We note that, as for the potential and kinetic energies of an oscillating pendulum, there is a phase shift between surface and fluid kinetic energies. After the impact, the interface will oscillate, implying several reversal of the flow direction through the time. The sum of the potential and curvature energies of the surface is the highest when the surface is largely deformed, creating a peak ridge or a dimple. At the same moment, there is a reversal of direction in the flow, the water velocity is low and the kinetic energy in the fluid is the lowest. At $t = 30ms$ (instant 1 in the figure 8.a), the drop impact has highly depressed the surface, and the surface starts to pull up the fluid. At this instant, the kinetic energy in the measurement volume is low and potential and curvature energies of the surface are larger. At $t = 40ms$ (instant 2 in the figure 8.a), the flow velocity is close to its maximum, the kinetic energy is large when compared to the surface energy and the surface is almost flat. Between $t = 50ms$ and $t = 60ms$ (instant 3 in the figure 8.a) the surface rises above its resting position, this backjet (or rebound) of the interface is caracterized by an increase in the surface energy, which reaches its maximum at $t = 70ms$.

5 Discussion and Perspectives

We have presented a novel extension of the Tomo-PTV technique to the estimation of the three dimensionnal velocity field in a free surface flow, together with the estimation of the topography of the interface. This technique allows us to track accurately particles at seeding densities comparable to the thresholds for tomographic PIV and to reduce greatly the number of ghost particles. Apart from the firsts $20ms$, the estimated topography matches well the independent estimation of surface topography provided by direct visualisations. Using 3D velocity field and topography, we produce a time resolved balance of energy in the surface and bulk flow. In the particular case of a drop impacting water interface at relatively large Weber number ($We = 300$), the extent of the cavity formed after the impact is such that it exceed our measurement field of view, imparting a loss of a part of the gravitationnal and curvature energies. The lack of vertical extent of

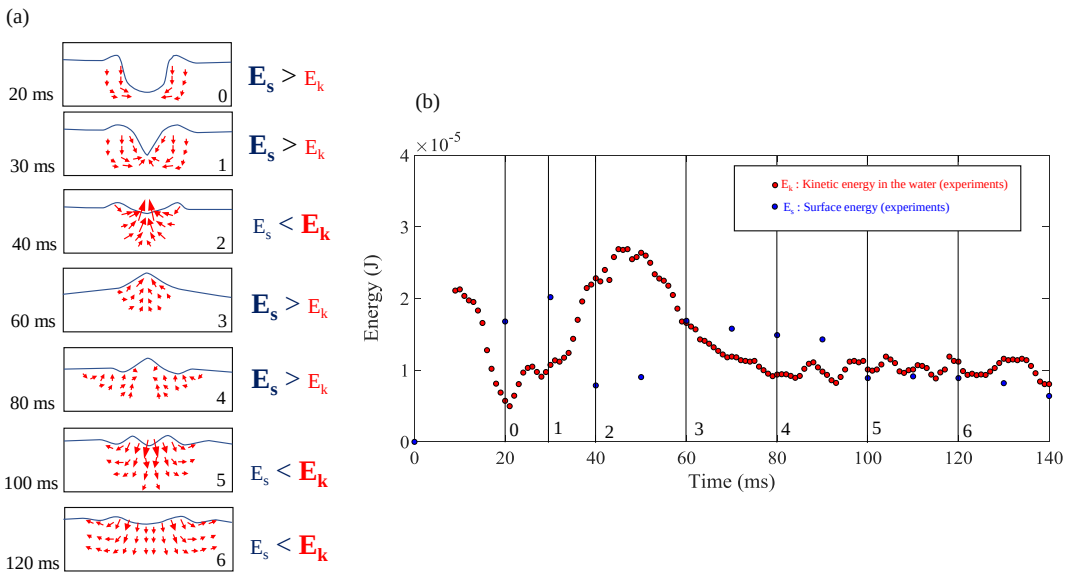

Figure 8: Temporal evolution of the energies in the surface and in the bulk flow below the interface. (a) We illustrate a cross section of the interface topography together with a cross section of the velocity field under the water interface for 6 instants (20, 30, 40, 60, 80, 100 and 120 ms). (b) Evolution of the energies balance between surface and fluid kinetic energies derived from the tomo-PTV experiment.

our measurement volume (from $z = -5mm$ to $z = +5mm$) was mainly due to the relative shallow depth of field provided by the choice of macro lens. The large decrease of particles concentration at the instant of impact, coming from both the large size of the droplet and its large velocity, results in a difficult estimation of velocities in the first 15 ms of the processing.

The energy balance presented here neglect some of the work of the pressure forces. In the future, we plan to derive a more complete and precise energy balance in a given control volume. The correct estimation of this complete energy balance necessitate to derive the 3D pressure field. Recent methods have succesfully proof their ability to estimate the pressure fields, by integrating its gradient on the domain of measurement of velocity fields (Tronchin et al. (2015)). The accuracy of pressure field estimation is however partially function of local uncertainties of velocity field. We have shown that the tomo-PTV/*STB* method is promising and could be used to study several surface flows, such as the wave field and vortical wake behind moving objects at the interface. The method should notably be well fitted to the experimental study of bulk flow movement and wave pattern generated by the leg strokes of water striders during a propulsion cycle. The resulting surface topography and underlaying fluid velocity should be thus compared to the previous experimental results and theoretical prediction (Hu et al. (2003), Bühler (2007), Gao and Feng (2010) and Steinmann et al. (2018)). This complete description of the flow and interface topography around animals moving at the interface and the resulting force and energy estimations should finally help to understand the unique aspects of the physics of the locomotion on water surface.

Acknowledgements

We thank Miguel Pineirua for his help with data analysis, and the Grant ARC Université de Tours/ Université de Poitiers for financing support.

References

Agbaglah G, Thoraval MJ, Thoroddsen ST, Zhang LV, Fezzaa K, and Deegan RD (2015) Drop impact into a deep pool: Vortex shedding and jet formation. *Journal of Fluid Mechanics* 764:764R1–764R12

Aureli F, Maranzoni A, Mignosa P, and Ziveri C (2011) An image processing technique for measuring free surface of dam-break flows. *Experiments in Fluids* 50:665–675

Bühler O (2007) Impulsive fluid forcing and water strider locomotion. *Journal of Fluid Mechanics* 573:211

Chatellier L, Jarny S, Gibouin F, and David L (2013) A parametric PIV/DIC method for the measurement of free surface flows. *Experiments in Fluids* 54

Cobelli PJ, Maurel A, Pagneux V, and Petitjeans P (2009) Global measurement of water waves by Fourier transform profilometry. *Experiments in Fluids* 46:1037–1047

Douxchamps D, Devriendt D, Capart H, Craeye C, MacQ B, and Zech Y (2005) Stereoscopic and velocimetric reconstructions of the free surface topography of antidune flows. *Experiments in Fluids* 39:533–551

Fouras A, Lo Jacono D, Sheard GJ, and Hourigan K (2008) Measurement of instantaneous velocity and surface topography in the wake of a cylinder at low Reynolds number. *Journal of Fluids and Structures* 24:1271–1277

Gao P and Feng JJ (2010) A numerical investigation of the propulsion of water walkers. *Journal of Fluid Mechanics* 668:363–383

Gilet T and Bourouiba L (2015) Fluid fragmentation shapes rain-induced foliar disease transmission. *Journal of the Royal Society Interface* 12

Gomit G, Chatellier L, Calluaud D, and David L (2013) Free surface measurement by stereo-refraction. *Experiments in Fluids* 54

Hu DL, Chan B, and Bush JWM (2003) The hydrodynamics of water strider locomotion. *Nature* 424:663–666

Joung YS and Buie CR (2015) Aerosol generation by raindrop impact on soil. *Nature Communications* 6:1–9

Leng LJ (2002) Splash formation by spherical drops. *Journal of Fluid Mechanics* 427:73–105

Michon GJ, Josserand C, and Séon T (2017) Jet dynamics post drop impact on a deep pool. *Physical Review Fluids* 2:1–13

Moisy F, Rabaud M, and Salsac K (2009) A synthetic Schlieren method for the measurement of the topography of a liquid interface. *Experiments in Fluids* 46:1021–1036

Ng I, Kumar V, Sheard GJ, Hourigan K, and Fouras A (2011) Experimental study of simultaneous measurement of velocity and surface topography: In the wake of a circular cylinder at low Reynolds number. *Experiments in Fluids* 50:587–595

Rein M (1993) Phenomena of liquid drop impact on solid and liquid surfaces. *Fluid Dynamics Research* 12:61

Rein M (1996) The transitional regime between coalescing and splashing drops. *Journal of Fluid Mechanics* 306:145–165

Schanz D, Gesemann S, and Schröder A (2016) Shake-The-Box: Lagrangian particle tracking at high particle image densities. *Experiments in Fluids* 57:1–27

Steinmann T, Arutkin M, Cochard P, Raphaël E, Casas J, and Benzaquen M (2018) Unsteady wave pattern generation by water striders. *Journal of Fluid Mechanics* 848:370–387

Thoraval MJ, Li Y, and Thoroddsen ST (2016) Vortex-ring-induced large bubble entrainment during drop impact. *Physical Review E* 93:1–10

Tronchin T, David L, and Farcy A (2015) Loads and pressure evaluation of the flow around a flapping wing from instantaneous 3D velocity measurements. *Experiments in Fluids* 56

Turney DE, Anderer A, and Banerjee S (2009) A method for three-dimensional interfacial particle image velocimetry (3D-IPIV) of an air-water interface. *Measurement Science and Technology* 20

Wildeman S (2018) Real-time quantitative Schlieren imaging by fast Fourier demodulation of a checkered backdrop. *Experiments in Fluids* 59:1–13

Yarin A (2006) DROP IMPACT DYNAMICS: Splashing, Spreading, Receding, Bouncing.... *Annual Review of Fluid Mechanics* 38:159–192

Zhang Y, Liu P, Qu Q, and Hu T (2019) Energy conversion during the crown evolution of the drop impact upon films. *International Journal of Multiphase Flow* 115:40–61